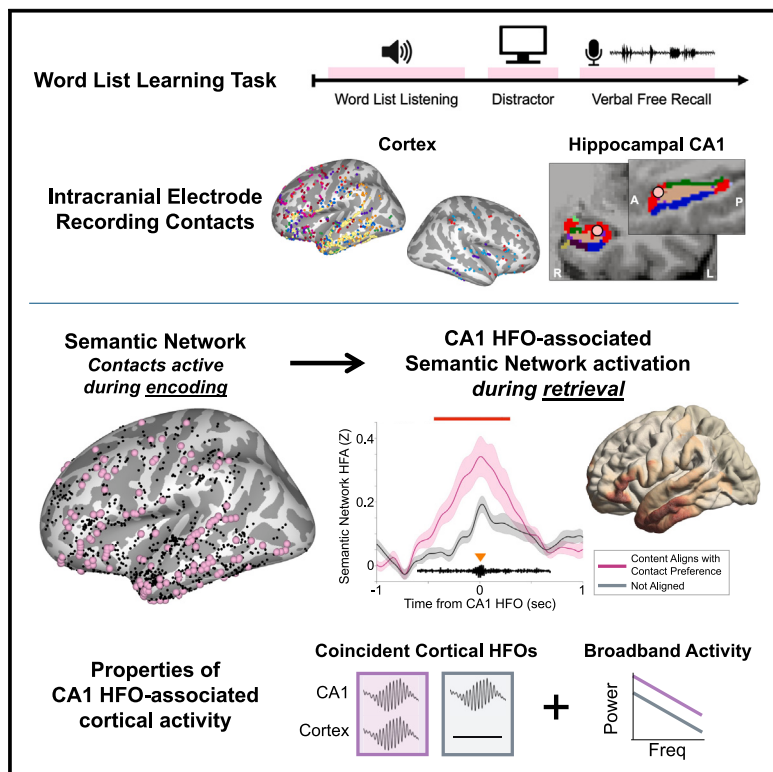


Hippocampal and cortical high-frequency oscillations orchestrate human semantic networks during word list memory

Graphical abstract



Authors

Akash Mishra, Serdar Akkol,
Elizabeth Espinal, ..., Elisabeth Freund,
Ashesh D. Mehta, Stephan Bickel

Correspondence

amishra4@northwell.edu (A.M.),
sbickel@northwell.edu (S.B.)

In brief

Cognitive neuroscience; Linguistics

Highlights

- Human hippocampal HFOs (hHFOs) increase during word list encoding and retrieval
- In retrieval, HFOs coincide with content-specific cortical semantic network activity
- A subset of hHFOs is temporally coincident with cortical HFOs
- Coincident HFOs are associated with increased broadband cortical activity



Article

Hippocampal and cortical high-frequency oscillations orchestrate human semantic networks during word list memory

Akash Mishra,^{1,2,7,*} Serdar Akkol,^{1,3,4} Elizabeth Espinal,^{1,3,5} Noah Markowitz,^{1,3} Gelana Tostaeva,^{1,3} Elisabeth Freund,^{1,3} Ashesh D. Mehta,^{1,2} and Stephan Bickel^{1,2,3,6,*}

¹Northwell, New Hyde Park, NY, USA

²Departments of Neurosurgery and Neurology, Zucker School of Medicine at Hofstra/Northwell, Hempstead, NY, USA

³Feinstein Institutes for Medical Research, Northwell Health, Manhasset, NY, USA

⁴Elmezzi Graduate School of Molecular Medicine, Manhasset, NY, USA

⁵Department of Psychological and Brain Sciences, Drexel University, Philadelphia, PA, USA

⁶Center for Biomedical Imaging and Neuromodulation, Nathan Kline Institute, Orangeburg, NY, USA

⁷Lead contact

*Correspondence: amishra4@northwell.edu (A.M.), sbickel@northwell.edu (S.B.)

<https://doi.org/10.1016/j.isci.2025.112171>

SUMMARY

Episodic memory requires the precise coordination between the hippocampus and distributed cortical regions. This may be facilitated by bursts of brain activity called high-frequency oscillations (HFOs). We hypothesized that HFOs activate specific networks during memory retrieval and aimed to describe the electrophysiological properties of HFO-associated activity. To study this, we recorded intracranial electroencephalography while human participants performed a list learning task. Hippocampal HFOs (hHFOs) increased during encoding and retrieval, and these increases correlated with memory performance. During retrieval, hHFOs demonstrated activation of semantic processing regions that were previously active during encoding. This consisted of broadband high-frequency activity (HFA) and cortical HFOs. HFOs in the anterior temporal lobe, a major semantic hub, co-occurred with hHFOs, particularly during retrieval. These coincident HFOs were associated with greater cortical HFA and cortical theta bursts. Hence, HFOs may support synchronization of activity across distributed nodes of the hippocampal-cortical memory network.

INTRODUCTION

Human memory depends on an intricate, bidirectional interplay between the hippocampus and the distributed cortical regions that contain memory representations. There is great interest in understanding the mechanisms by which these distant regions communicate because this may elucidate the processes that underlie human memory function and represent potential therapeutic targets for the amelioration of memory impairment. One candidate mechanism underlying this brain-wide, multi-areal coordination are high-frequency oscillations (HFOs), which represent specific patterns of synchronized neuronal firing.^{1,2}

Several rodent studies have implicated physiological hippocampal HFOs (hHFOs) as a key mechanism supporting a two-stage framework of memory. In this framework, information is initially encoded in the hippocampus and consolidated in the cortex; then, during memory retrieval, the hippocampus reactivates these same memory-containing cortical sites.^{2–4} More recent studies using intracranial electrodes in human participants have detected 70–180 Hz HFOs that show similar dynamics and characteristics to physiological rodent HFOs.^{5,6} To support a function of human hHFOs in episodic memory func-

tion, hHFOs have been associated with increases in local neuronal population firing of specific memory-containing cortical regions during memory encoding and recall.^{5,7,8} These increases in cortical activity have often been quantified using broadband (without any distinct bursts of oscillatory activity) high-frequency activity (HFA).^{3,9} Intriguingly, more recent studies have identified cortical HFOs that are temporally coincident and morphologically similar (in frequency and duration) to hHFOs.^{5,6,10} Hence, the literature suggests that HFO-associated cortical HFA contains both oscillatory (cortical HFOs) and broadband components. There are several notable gaps in our knowledge of these mechanisms. First, the connection between HFOs and memory performance in humans, including the specific interaction of HFOs with cortical regions containing task-specific memory representations, requires further support. Second, because studies have identified hHFO-associated cortical activation consisting of both broadband HFA and cortical HFOs, it is imperative to further study the relationships between these two activity profiles. Finally, few studies have described the relationship between HFOs and lower frequency oscillations, but a synergy between these two mechanisms may be suggestive of periods of more optimal binding of activity.^{11–13} Knowledge derived from this



study would clarify how HFOs coordinate brain activity during human memory function and how HFOs interact with other mechanisms (oscillatory and non-oscillatory; high and low frequency) to support these processes.

Word list learning is a cognitive process that requires coordination of distributed brain regions to process and encode words. Because multi-regional synchrony is involved, HFOs may coordinate this process. Recent studies have identified a semantic processing network consisting of precisely-coordinated cortical regions that are activated during speech perception.^{14–16} This network reflects an intricate hierarchical processing ensemble that spans the primary auditory cortex and widespread cortical regions. The level of comprehension and complexity increases as higher-order regions are recruited (e.g., syllables to words to sentences).^{17–19} This large, distributed cortical network involves frontal, anterior and posterior temporal, and parietal regions.^{15,16,20} Notably, the anterior temporal lobe (ATL) may serve as a critical interface for this semantic processing network, as it coordinates semantic processing^{21–23} and serves as the interface between the posterior temporal lexical-semantic areas and frontal cortex regions.²⁴ Therefore, the semantic network and the ATL represent brain areas that require precise coordination during word list processing and memory and hence, represent a unique medium to investigate the function of HFOs.

We used an auditory word list learning task with verbal free recall to assess the relationship between hippocampal and cortical HFOs and the activation of semantic networks during encoding and recall. We recorded intracranial electroencephalography (iEEG) from individuals undergoing invasive neuromonitoring for the treatment of intractable epilepsy to gain rare neural recordings of memory and semantic networks with high spatial and temporal resolution. We show that hHFOs are associated with both cortical HFOs and broadband HFA in specific areas of the semantic processing network, and the profile of this activity is influenced by memory content. Further, a subset of hippocampal-ATL co-HFOs are coincident with 3–5 Hz ATL cortical oscillations. These results extend our understanding of HFOs to the dynamic activation of semantic networks and elucidate the mechanisms by which hHFOs, cortical HFOs, and low-frequency oscillations coordinate the hippocampal-cortical memory network.

RESULTS

Behavioral results

Nine participants performed a word list learning task with verbal free recall (Figures 1A and S1). Electrode coverage and clinical information for participants are provided in Tables S1 and S2. Of note, all participants had at least one contact in each area of interest (hippocampus, semantic network, and ATL), and most participants did not have evidence of significant verbal memory impairment on neuropsychological testing. On average, participants recalled 4.1 ± 2.0 words (of 12 total) per trial across 1.6 ± 0.8 recall events per trial (median recall duration was 2.4 s). Participants showed a trend toward recalling more words in trials where words were assembled into sentences (sentence condition) compared to when they were not (non-sentence condition) (Wilcoxon signed-rank test, $W = 1.953$, $p = 0.051$).

hHFO rate is modulated by encoding of word lists and subsequent free recall

We identified hHFOs from the local field potentials (LFPs) of hippocampal contacts located within (or immediately adjacent to) the CA1 subfield (Figures 1C and S2). Across 9 participants, we identified 5,093 hHFOs during all task periods (encoding, distractor, and recall) (Figures 1D and 1E). The median peak hHFO frequency across all participants was 113 Hz (Figure 1F), and the median inter-hHFO interval duration was 1.3 s (Figure 1G).

Since hHFOs may coordinate neural activity during encoding and recall, we investigated hHFO rate during these task periods. First, we created peri-event time histograms (PETH) of hHFOs during word list presentation ($n = 7$ participants) (Figure 2A; results from two participants who performed the task with a different inter-stimulus interval duration is shown in Figure S3). After removal of 33 trials where external interruption or mis-click occurred, we assessed 177 word presentation trials (8-s word list presentation, followed by a 2-s rest period). The hHFO rate was increased starting 1,400 ms after presentation onset and decreased 800 ms after presentation offset ($p < 0.001$, permutation test) (Figure 2A). Of note, hHFO rate did not significantly differ between the presentations of sentence and non-sentence word lists (Figure S4). Next, we assessed hHFO dynamics during memory retrieval by generating a PETH locked to verbal free recall onsets. hHFO rate was transiently increased 1,000 ms prior to recall onset for roughly 200 ms ($n = 342$ trials; $p = 0.037$, permutation test) (Figure 2B). Importantly, hHFO rate was not reliably modulated by vocalizations captured during the task period, hence diminishing the possibility that gross movements or muscle artifacts influence hHFO detection (Figure S5).

As hHFOs represent a potential marker for effective memory processes, increased hHFO rates during memory encoding and recall may be associated with improved memory performance. We separated trials into two groups based on whether participants executed a good response (number of words recalled in the trial was above the participant's median across all trials) or poor response (below or equal to the median). Across participants, the mean number of words recalled for good recalls was 5.7 ± 1.8 words (139 events) compared to 3.2 ± 1.4 for poor recalls (203 events). We then compared hHFO dynamics prior to recall onset for good and poor responses. hHFO rate was higher for recalls that corresponded to good response trials in the 1,000 ms window prior to verbal free recall compared to poor responses ($p = 0.031$, permutation test) (Figure 2C). Finally, we examined the relationship between hHFO rate during encoding/recall on memory performance on the group level (one rate value per participant). hHFO rate during the word list presentation period was higher for good response trials (0.222 hHFOs/second) compared to poor response (0.167 hHFOs/second) (two-tailed Mann-Whitney $U = 109$, $n_1 = n_2 = 9$, $p = 0.0379$) (Figure 2D). This group-level relationship holds a trend when assessing hHFO rate in the window around free recall onset (-2 to $+0.5$ s relative to free recall onset; two-tailed Mann-Whitney $U = 39$, $n_1 = n_2 = 9$, $p = 0.0547$) (Figure 2E). Hence, hHFOs may reflect hippocampal activity that relates to memory function during word list encoding and retrieval.

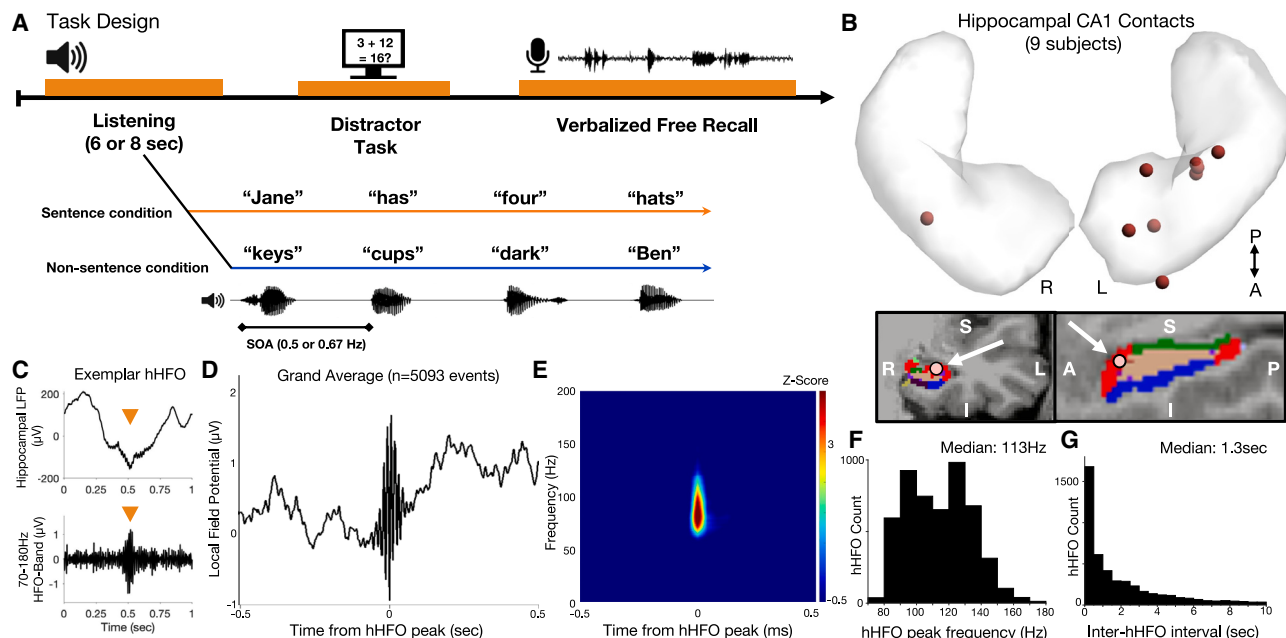


Figure 1. Experimental design and hippocampal high-frequency oscillation (hHFO) detection

- (A) Experimental design and example stimuli presented to participants. Participants listened to a list of 12 words assembled into either 3 sentences (of 4 words each) or a randomized word list. Then, after an arithmetic distractor task, participants were asked to freely recall as many words as possible. Sentence and non-sentence trials were randomized and interleaved for a total of 30 trials.
- (B) (Top) Hippocampal depth electrode selection across all participants. One point represents an individual participant. (Bottom) Representative structural reconstruction of hippocampal depth electrodes in one participant in coronal (left) and sagittal (right) views; white arrows denote CA1 recording site implemented for hHFO detection analysis. Red parcellation indicates CA1 subregion. (See Figure S2 for similar reconstructions for other participants).
- (C) Example of hHFOs as they appear in (top) the raw hippocampal local field potential and (bottom) the 70–180 Hz frequency range.
- (D) Grand average peri-hHFO field potential locked to hHFO peak for $n = 5,093$ events from nine participants.
- (E) Wavelet spectrogram locked to hHFO peak for $n = 885$ hHFOs from one representative participant. Warmer colors indicate a higher spectral power in that frequency-time combination.
- (F) Distribution of hHFO peak frequencies and (G) inter-hHFO interval for $n = 5,093$ hHFOs from nine participants.

hHFOs reactivate functional semantic network regions during free recall

hHFOs may facilitate the interaction between the hippocampus and memory-containing cortical regions. Hence, hHFOs during the recall portion of a word list learning task may activate cortical regions that were previously engaged during word list encoding. We first defined the cortical semantic network by assessing HFA during word list presentation in all cortical contacts (Figure S1). We identified 150 contacts that exhibited higher HFA during the listening of sentence compared to non-sentence word lists (“sentence-responsive”) and 79 cortical contacts that showed the opposite HFA profile (“non-sentence-responsive”) (false discovery rate [FDR]-corrected $p < 0.01$, permutation test). Figure S6 depicts the difference in HFA activation between preferred and non-preferred trials across all contacts. These identified contacts were distributed across several higher-order cortical regions, which aligns with prior studies that have defined this large cortical semantic network (Figure 3A).

We then assessed the interaction between hHFOs and HFA in this semantic network during recall periods. We observed an hHFO-associated HFA increase in cortical contacts when there was congruence between the electrode preference and trial

type (“preferred” trial-electrode combination) compared to when there was no congruence (“non-preferred” combination) ($p = 0.031$, cluster-based permutation test) (Figure 3C). This effect is also readily visible at the single contact level (sentence-responsive contact: $n = 180$ words in sentence list, $n = 168$ words in non-sentence list; two-sample Wilcoxon rank-sum $z = 2.238$, $p = 0.025$; reactivation: cluster-based permutation test clustering time bins, $p = 0.018$) (Figure 3B). To evaluate the spatial distribution of this effect, we calculated the effect size of hHFO-locked HFA activation between preferred and non-preferred trials in a 500 ms window around hHFO peak (Figures 3D and S7; spectrograms in Figure S8). Temporal lobe contacts displayed the highest difference between preferred and non-preferred hHFO-locked activation.

hHFO-associated ATL HFA: Coincident cortical HFO or broadband HFA?

Prior studies have identified hHFO-coincident ATL HFOs in a word association task.^{5,7} Similarly, we noted a prominent hHFO-locked HFA increase in the ATL (Figure 3D) with a spectral peak in the HFO range. Hence, we aimed to replicate these findings and further investigate the relationship between broadband HFA and cortical HFO activity in this region.

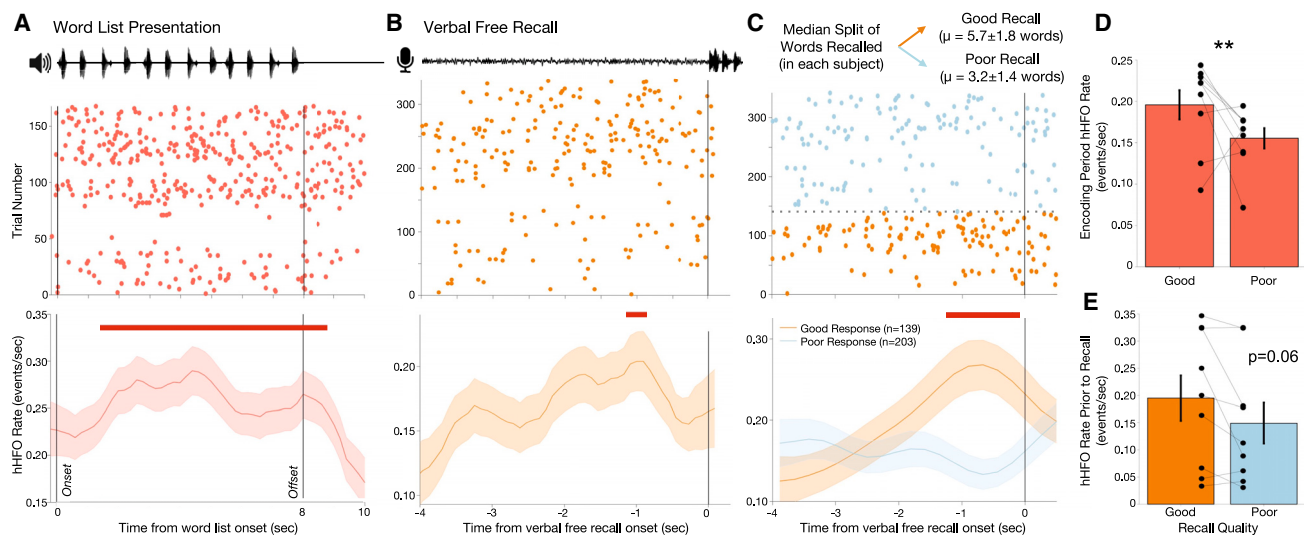


Figure 2. Hippocampal high-frequency oscillation (hHFO) dynamics during word list presentation and free recall

- (A) hHFO raster plot and peri-event time histogram (PETH) time-locked to the onset of word list presentation ($n = 168$ trials across 7 participants), depicting a sustained increase in hHFO rate in response to word list presentation compared to baseline that subsequently diminishes after offset of word presentation (vertical line). Two participants were removed from this analysis due to variation in word presentation frequency but demonstrated a similar hHFO rate increase (Figure S3). Red line indicates significance at $p < 0.05$ (permutation test compared to shuffled hHFO times in the 2-s post-trial resting period). Shaded areas represent one bootstrap standard error computed over hHFO events.
- (B) hHFO raster plot and PETH time-locked to the onset of distinct recall vocalizations ($n = 338$ trials across 9 participants), indicating a transient response-locked increase in hHFO rate. Red line indicates significance at $p < 0.05$ (permutation test shuffling hHFO times across this PETH epoch). Shaded areas represent one bootstrap standard error computed over hHFO events.
- (C) hHFO raster plot and PETH time-locked to onset of distinct recall vocalizations. Data are median split by the number of words recalled during that trial where “good response” ($n = 139$ trials) was a trial where the participant recalled more than their median number of recalled words across trials and a “poor response” was equal to or below the median ($n = 203$ trials). Red line denotes significance at $p < 0.05$ (cluster-based permutation test clustering across time, $p < 0.05$). Shaded areas represent one bootstrap standard error computed over hHFO events.
- (D) Mean hHFO rate during the encoding phase for trials that contained a good response and poor response. Each point represents the mean hHFO rate per participant, and lines connect data for each participant. Error bar depicts standard deviation across participant. Stars denote significance at $p < 0.05$ (Mann-Whitney U test).
- (E) Mean hHFO rate during the 2 s window prior to onset of verbal free recall in trials that contained a good response and poor response. Each point represents the mean hHFO rate per participant, and lines connect data for each participant. Error bar depicts standard deviation across participants.

We first assessed HFA increases locked to hHFOs in the recall period (500 ms window centered on hHFO peak) across all cortical contacts (Figure 4A; effect size in Figure S9) and identified a prominent increase in the area corresponding to the ATL. To investigate this further, we then isolated ATL contacts ($n = 218$) using anatomical reference and excluded 22 contacts that overlapped with the semantic network (Figure 4B). Not surprisingly, hHFOs were associated with a significant increase in ATL HFA ($p < 0.001$, cluster-based permutation test) (Figure 4C), maximally at the time of the hHFO peak. Spectral analysis of the hHFO-locked cortical activity showed a spectral peak in the 80–120 Hz range as well as an increased broadband HFA (Figure 4D). Since the spectral peak was found at the expected frequency range of cortical HFOs, we then conducted an HFO detection analysis for all ATL contacts. Detected ATL HFOs were found to have peak frequencies predominantly within the 80–140 Hz range (Figure 4E) but centered around 114 Hz (Figure 4F) and with a median inter-HFO interval of 1.9 s (Figure 4G).

We next assessed the coincidence of HFOs by computing a cross-correlogram between hHFOs and ATL HFOs during memory retrieval. There was significant coincidence ($p < 0.01$, permu-

tation test), with a mean difference of ATL HFO peak relative to hHFO peak of 14 ms (Figure 5A). Further, the proportion of hHFOs that were associated with an ATL HFO increased 700 ms prior to verbal free recall and was sustained until the onset of free recall ($p = 0.0354$, permutation test) (Figure 5B). Hence, hHFOs transiently increase in the 1-s window prior to recall (Figure 2B), and these hHFOs are more likely to co-occur with ATL HFOs. Interestingly, compared to ATL HFOs that were not coincident with an hHFO, hippocampal-ATL co-HFOs in the recall period were of higher frequency (median 119 Hz compared to 113 Hz; two-tail Wilcoxon rank-sum $z = 5.868$, $p < 0.001$) and shorter duration (80 ms compared to 96 ms; two-tail Wilcoxon rank-sum $z = 7.665$, $p < 0.001$) (Figure S10).

The presence of hHFO-evoked cortical HFA raises an important methodological question: are hHFO-locked increases in HFA a product of synchronous ATL HFOs, broadband HFA, or both? ATL HFOs during the recall period that were coincident with an hHFO exhibited a greater increase in ATL HFA compared to those not coincident with an hHFO ($p < 0.001$, cluster-based permutation test) (Figure 5C). Both hHFO-coincident and non-coincident ATL HFOs exhibited a significant increase in HFO

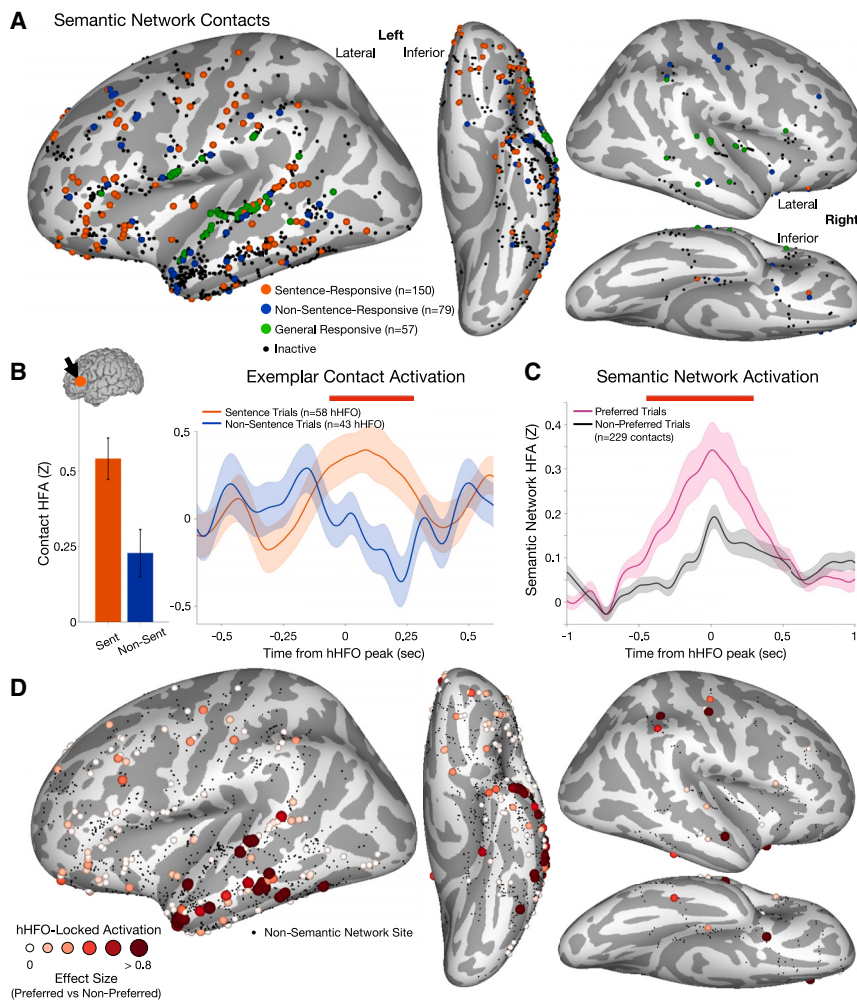


Figure 3. Hippocampal high-frequency oscillation (hHFO)-locked activation of the semantic network

(A) Left lateral (left), left inferior (middle), right lateral (right upper), and right inferior (right lower) views on inflated brains of locations of sentence-responsive (orange, $n = 150$), non-sentence-responsive (blue, $n = 79$), and general semantic-responsive (green, $n = 57$) contacts on an inflated brain. (Also see increase in HFA during preferential word list presentation in Figure S6).

(B) Peri-hHFO HFA responses in an exemplar electrode. (Left) HFA response during word presentation by sentence (Sent) and non-sentence (Non-Sent) trial ($n = 15$ trials and $n = 180$ words each; error bars denote standard deviation across trials, stars denote significance at $p < 0.05$, Wilcoxon rank-sum test); (inset) location of the selected electrode; (right) HFA response locked to hHFOs that occurred in the recall period when participants recalled words from either sentence ($n = 58$ hHFOs) or non-sentence trials ($n = 43$ hHFOs). Red bar represents significant time bins at $p < 0.05$ (cluster-based permutation test clustering across time). Shaded areas represent one standard error computed over hHFO events.

(C) HFA time-locked to peak of hHFO events that occurred during recall of trials that aligned with the contact's preference as compared to when they did not. Red line denotes significant time bins at $p < 0.05$ (cluster-based permutation test, $n = 212$ bipoles). Shaded areas represent one standard error computed across contacts. (Also see spectrogram of this analysis in Figure S8).

(D) Activation effect size (in Cohen's d) for semantic network contacts (combining sentence-responsive and non-sentence-responsive contacts) comparing peri-hHFO HFA activation during the recall period of preferred versus non-preferred trials.

Darker colors and larger electrode sizes depict larger effect sizes.

power (especially between 80 and 140 Hz), but only co-HFOs exhibited a significant power increase above 140 Hz ($p = 0.032$, cluster-based permutation test) (Figure 5D; spectrograms in Figure S11). This suggests that co-HFOs are associated with increased broadband ATL HFA that is less prevalent when ATL HFOs do not co-occur with hHFOs.

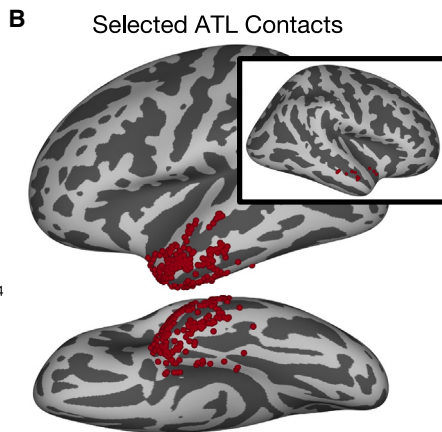
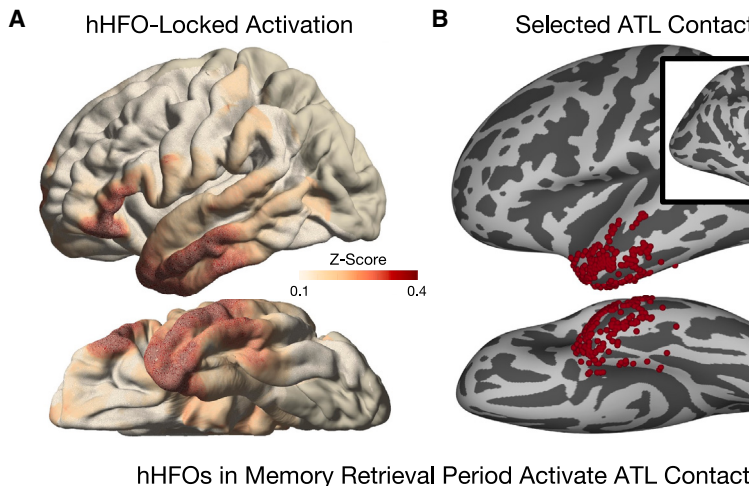
Coincident hippocampal-cortical HFOs across the semantic network

Co-HFOs may serve as a precise mechanism for synchronizing the activity of multiple nodes within the hippocampal-cortical memory network. Hence, we examined the impact of co-HFOs on the recruitment of cortical regions, with an emphasis on elucidating the dynamics of hHFOs, ATL HFOs, and semantic network HFOs (here, combining sentence-responsive and non-sentence responsive contacts). First, hippocampal-ATL co-HFOs during the recall period exhibited a greater increase in semantic network HFA compared to hHFOs that were not coincident with an ATL HFO ($n = 491$ hippocampal-ATL co-HFOs, $n = 276$ non-coincident hHFOs) ($p < 0.001$, cluster-based permutation test) (Figure 5E). This may indicate that

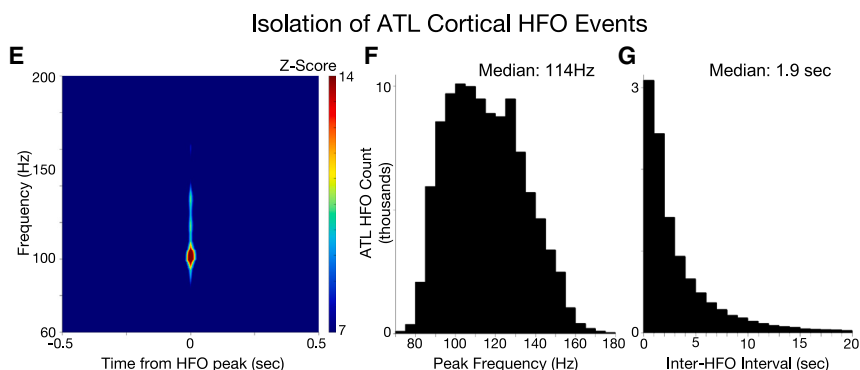
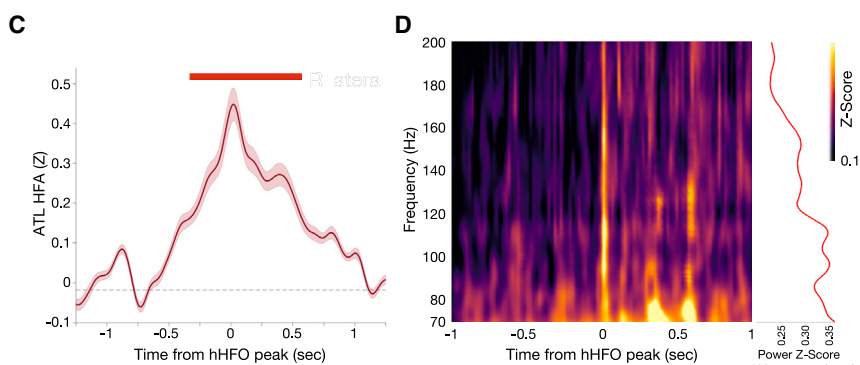
hippocampal-ATL co-HFOs more optimally recruit the cortical semantic network.

However, as with above, this result may be a product of hippocampal-semantic network co-HFOs. To investigate this possibility, we identified semantic network HFOs and repeated the same analysis as in Figure 5E but after removing all hHFOs where there was a coincident semantic network HFO. We no longer found a significant semantic network HFA increase resulting from hippocampal-ATL co-HFOs ($p = 0.293$, cluster-based permutation test; $n = 157$ hHFOs with coincident ATL HFOs and $n = 147$ hHFOs without coincident ATL HFOs) (Figure 5F). Hence, it is probable that the observed effect of hippocampal-ATL co-HFOs on semantic network HFA is influenced by hippocampal-semantic network co-HFOs.

We then investigated whether semantic network HFOs exhibit spatial specificity during recall. We assessed whether there was an increased incidence of cortical HFOs for trials where the hHFO and semantic network contact (Figure 3) showed congruence in preference (i.e., an hHFO that occurred during free recall of a sentence trial and coincident semantic network HFO occurring in a sentence-responsive contact and



hHFOs in Memory Retrieval Period Activate ATL Contacts



the same for non-sentence trials/contacts) compared to when there was no congruence (i.e., hHFO in a sentence trial and semantic network HFOs in a contact that had preference for non-sentence trials or vice versa). The rate of triple co-occurrence of HFOs in the hippocampus, ATL, and semantic network contact was increased when there was alignment between recall content and contact preference compared to when there was no alignment (2.1% of hippocampal-ATL-semantic network contact pairs showed coincidence for aligned preference compared to 1.9% of pairs showing coincidence for non-aligned preference, $\chi^2(1, n = 346,182) = 18.802, p < 0.001$). This indicates spatial specificity of cortical HFOs based on the content of recall.

Figure 4. Properties of anterior temporal lobe (ATL) cortical high-frequency oscillations

(A) Left lateral (top) and left inferior (bottom) views of normalized brains with overlaid heatmap representing regions of increased HFA increase locked to peaks of hippocampal high-frequency oscillations (hHFOs) within the recall period across all contacts. Darker colors represent increased HFA, and uncolored regions represent no electrode coverage in the region.

(B) Left lateral (top), left inferior (bottom), and right lateral (inset) views on inflated brains depicting the location of $n = 196$ anterior temporal lobe contacts across participants. Contacts were selected on participant-specific imaging, and precise location may be distorted in the transfer to standardized space.

(C) Increase in HFA, locked to peaks of hHFOs within the recall period for $n = 196$ ATL contacts.

Red line denotes significant time bins at $p < 0.05$ (cluster-based permutation test against pre-hHFO baseline). Shaded areas represent one standard error computed across ATL contacts.

(D) (Left) Wavelet spectrogram of ATL high-fre-

quency power locked to hHFOs alongside (right)

mean power in the 40 ms window centered

around hHFO peak for each frequency repre-

sented in the spectrogram depicting an in-

crease in the 90–120 Hz range. Warmer colors

represent increased power.

(E) Wavelet spectrogram time locked to ATL HFO peak ($n = 7,773$ events from one participant with $n = 12$ ATL contacts). Warmer colors indicate a

higher spectral power in that frequency-time

combination.

(F) Distribution of peak frequencies and (G) and inter-HFO duration for all detected ATL HFOs ($n = 108,510$ events in $n = 196$ contacts across $n = 9$ participants).

Hippocampal-ATL co-HFOs are associated with low-frequency oscillations

Thus far, this analysis has probed the relationship between HFOs and HFA, but a key missing component is the investigation of lower frequencies. We investigated this by examining relationships

between HFOs and 2–12 Hz neural activity. Hippocampal-ATL co-HFOs ($n = 1184$) were most associated with an increase in ATL 3–5 Hz power compared to ATL HFOs that were not coincident with an hHFO ($n = 14,759$) ($p = 0.016$, permutation test) (Figure 6A). This low-frequency power increase was roughly coincident with the ATL HFO peak ($p = 0.003$, permutation test) (inset, Figure 6A). As this analysis was across trials, we then confirmed the presence of low-frequency oscillations in single trials around the hippocampal-ATL co-HFOs. Once again, detected oscillations showed a peak frequency between 3 and 5 Hz (Figure 6B). Finally, to more precisely assess the temporal relationship between hippocampal-ATL co-HFOs and 3–5 Hz oscillations, we constructed a cross-correlogram between 3 and 5 Hz oscillation

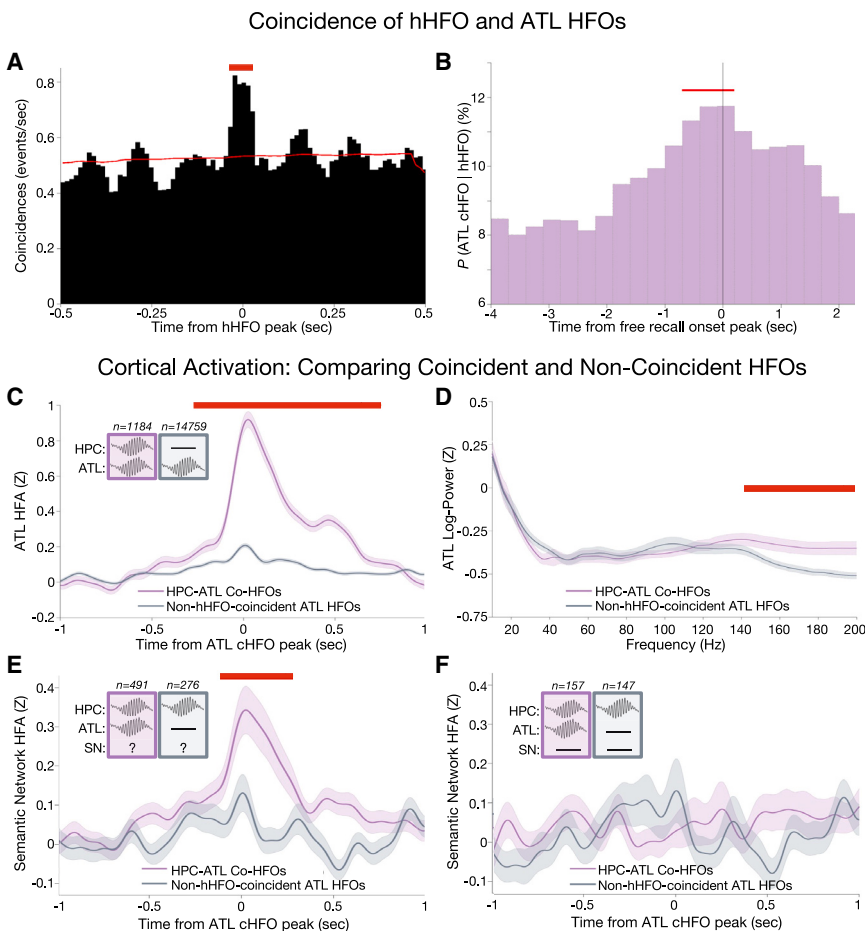


Figure 5. High-frequency oscillation (HFO)-locked activity across the hippocampus (HPC), anterior temporal lobe (ATL), and other semantic areas (SN)

(A) Cross-correlograms between ATL HFOs ($n = 15,943$ across $n = 196$ ATL contacts) and hippocampal HFOs (hHFOs) ($n = 772$ across $n = 9$ hippocampal contacts) within the recall period across $n = 9$ participants. Red line denotes significant time bins at $p < 0.05$ (permutation test with jittered ATL HFO timing), indicating high coincidence.

(B) Joint probability of coincident hippocampal-ATL co-HFO as a function of time relative to verbal recall onset. Red line denotes significant time bins at $p < 0.05$ (permutation test with jittered cortical HFO timing). A significant increase is present within 1 s window prior to verbal recall onset.

(C) ATL HFA locked to peak of ATL HFO in the recall period separated by whether the ATL HFO was coincident with an hHFO ($n = 1184$) or not ($n = 14759$). Red line denotes significant time bins at $p < 0.05$ (cluster-based permutation test). Shaded area represents standard error computed across ATL HFO events. (See spectral profile of this difference in Figure S11).

(D) High-frequency spectral profile of ATL HFOs in the recall period that were associated with hHFOs compared to that are not coincident with hHFOs. Red line denotes significant frequencies at $p < 0.05$ (cluster-based permutation test). Shaded area represents one standard error computed across ATL HFO events.

(E) HFA in semantic network contacts, locked to peaks of hHFOs in the recall period by whether the hHFO was associated with an ATL HFO ($n = 491$) or not associated ($n = 276$). Red line denotes significant time bins at $p < 0.05$ (cluster-based permutation test). Shaded areas represent one standard error computed across HFO events.

Significant time bins at $p < 0.05$ (cluster-based permutation test). Shaded areas represent one standard error computed across HFO events.

(F) Same as in (E) but with all hHFO epochs containing a coincident semantic network HFO removed. Shaded areas represent one standard error computed across HFO events.

peaks and the peaks of ATL HFOs that were and were not coincident with an hHFO. Hippocampal-ATL co-HFOs exhibited co-occurrence with ATL 3–5 Hz oscillations at a higher rate compared to ATL HFOs that were not associated with an hHFO ($p = 0.002$, cluster-based permutation test) (Figure 6C). On average, the 3–5 Hz oscillation peak was delayed by 109 ms relative to the hHFO-coincident ATL HFO peak. This is suggestive of a potential relationship between hippocampal-ATL co-HFOs and low-frequency oscillations in the ATL.

DISCUSSION

Memory formation and retrieval involves a precise hippocampal-cortical coordination, and HFOs may support this process. We investigated this possibility by using intracranial recordings from the human hippocampus and widespread cortical regions while participants performed a word list learning task. We show that, during encoding and recall, the rates of hHFOs increased, and the magnitude of these increases were correlated with recall performance. During memory retrieval, hHFOs were associated with activation of specific cortical regions based on

recall content. In the ATL, a major semantic hub, hHFO-associated cortical activity contained both oscillatory (cortical HFO) and broadband HFA components. Finally, hippocampal-ATL co-HFOs were more coincident with low-frequency (3–5 Hz) oscillations than non-coincident ATL HFOs. Taken together, we replicate prior findings in supporting a function of hHFOs during word list encoding and retrieval^{26,27}; add support for congruence in the function and mechanisms of hHFOs across memory tasks in awake humans; and describe a complex interplay between hHFOs, cortical HFOs, broadband HFA, and low-frequency cortical oscillations in the semantic network that may coordinate brain activity underlying word list memory.

HFOs reflect highly synchronized patterns of neuronal activity that may be involved in coordinating activity across the hippocampus and cortex.²⁸ Hence, during encoding and recall, hHFOs may engage cortical regions that contain memory representations.⁶ An increase in hHFO rate during encoding likely reflects increased binding of hippocampal-cortical activity and strengthening of memory representations. Similarly, during retrieval, increased hHFO rate may indicate heightened activation of relevant memory traces. Increases in hHFO rate during

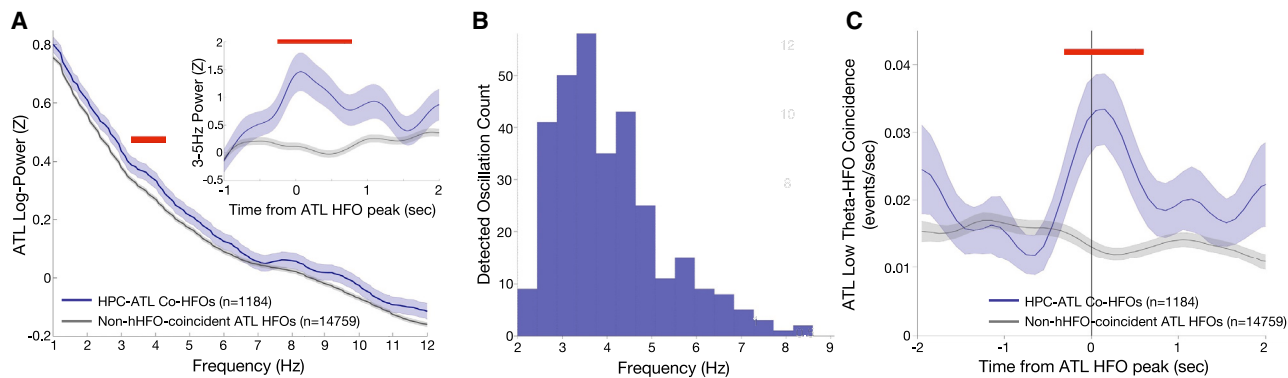


Figure 6. Relationship between cortical HFOs and theta oscillations

(A) Low-frequency spectral profile of anterior temporal lobe (ATL) activity locked to peak of ATL HFOs that were coincident (co-HFO; $n = 1,184$) and not coincident with an hHFO ($n = 14,759$). Red line denotes significant frequencies at $p < 0.05$ (cluster-based permutation test). Shaded areas represent one standard error across ATL HFO events. (Inset) Power in the 3–5 Hz low theta frequency range across time when locked to peak of ATL HFOs occurring in the recall period. Red line denotes significant time bins at $p < 0.05$ (cluster-based permutation test). Shaded areas represent one standard error across ATL HFO events.

(B) Distribution of peak frequency of detected low-frequency oscillations around ATL HFOs that were coincident with an hHFO.

(C) Cross-correlograms between peak of ATL HFOs that were coincident with hHFOs during the recall period and peak of ATL theta oscillations. Red line denotes significant time bins at $p < 0.05$ (cluster-based permutation test); 3–5 Hz oscillations occurred at a peak lag of 109 ms relative to coincident ATL HFOs. Shaded areas represent one standard error computed across cortical 3–5 Hz peak events.

successful encoding and retrieval have been identified previously in awake humans,^{3,26} and our findings align with these studies, as we identified increases in hHFO rate during both word list presentation and prior to free recall onset, and the magnitude of hHFO rate increase was higher when more words were recalled.

The auditory presentation of a set of words engages an assembly of interconnected cortical nodes that includes lower-order primary auditory cortical regions and higher-order regions involved in extracting rich semantic information.¹⁴ It is possible that these higher-order regions may contain word list memory representations, which hHFOs may engage. Here, we isolated contacts located in the semantic network based on their activity during encoding, including identifying sentence-preferring and non-sentence-preferring contacts. We found these contacts to be located in widespread frontal and cortical regions, similar to other studies that have described human semantic networks.^{16,20} We examined the relationship between hHFO and activity in this network during word list memory retrieval using broadband HFA, as this is the part of the iEEG signal that best correlates with neuronal population spiking.^{29,30} hHFO-associated increases in HFA have been previously described in visual processing regions,^{3,10} the default node network,⁹ and in sleep states, more dispersed cortical networks.³¹ We found that hHFOs during retrieval were associated with increased cortical HFA, and the magnitude of activation showed specificity for recall content. Hence, these findings link the semantic processing and word list memory literatures; further, it suggests that HFOs may serve as a linking mechanism between the two. It is interesting to note that the cortical HFA increases precede the hHFO peak by 400 ms. This finding supports a hypothesis that the cortex initiates memory retrieval by biasing hippocampal activity to generate hHFOs, which then function to reciprocally activate specific cortical memory representations.^{32–34} To this end,

a limitation of our recording technique is that it was not feasible to establish causal relationships between brain regions in the context of information exchange. Future studies should assess this relationship by using more granular recording methods (e.g., single unit recordings).

We next expanded our analysis to the ATL. This was motivated by finding that the ATL was one of the most activated areas in our data-driven hHFO-locked cortical HFA analysis and prior studies that have described a role of hHFOs in the activation of specific ATL neuronal assemblies during word association tasks.³⁵ Although the exact function of the ATL is still largely unknown, the hub-and-spoke theory suggests that this region facilitates the activation of individual semantic processing nodes to effectively retrieve higher order semantic concepts.³⁶ We found that hHFOs during the recall period were associated with coincident increases in ATL HFA, which consisted of both broadband HFA and cortical HFOs. Cortical HFOs are often temporally coincident with hHFOs and may play a role in the reinstatement of cortical memory representations.^{6,10} In support of this hypothesis in the domain of verbal memory, word association studies have shown temporal cortex HFOs to contain specific neuronal firing patterns that are indicative of memory representation activation.³⁵ We also found that 7.4% of ATL HFOs during the retrieval period were coincident with an hHFO. This is slightly lower than a similar study that reported 20% of association cortex HFOs co-occurring with hHFOs in rodents.³⁷ There may be several factors that may drive this discrepancy: poor proximity of recording contacts to HFO-generating nodes³⁸; suboptimal detection parameters for HFOs²⁵; and/or co-HFO rates are lower in humans compared to rodents. Cortical HFOs were of similar duration and frequency compared to hHFOs, but ATL HFOs that were coincident with an hHFO were of higher frequency and shorter duration compared to ATL HFOs that were not coincident with hHFOs. We speculate that this may be due to

different subtypes of cortical HFOs or that inter-areal communication via co-HFOs requires HFOs to be similar in frequency and/or duration. Next, we find that, even when the increase in hHFOs prior to recall is controlled for, hippocampal-ATL co-HFOs increase in coincidence prior to recall. Hence, ATL HFOs are not exclusive to periods of hHFOs, but their coincidence increases in periods of memory retrieval. Furthermore, hippocampal-cortical co-HFOs are more likely to occur in regions that were previously engaged during content encoding, indicating that the content of recall influences the presence of semantic network HFOs. Taken together, cortical HFO networks exist independently of hHFOs, but hippocampal-cortical HFO coincidence occurs in times where more optimal binding of activity is required. This supports the theory presented by Dickey et al.⁶ One critical piece of this puzzle that is still missing is the causality of this relationship. Intriguingly, it is possible that the hippocampus itself is not the primary (or “driving”) oscillator. This “cortical-centric” approach strays from prior human HFO studies, which have predominantly focused on hHFOs. Future study with more expansive spatial sampling of brain activity is needed to elucidate this potential relationship.

The precise relationship between human cortical HFOs and broadband HFA was previously not well understood. Here, we show that hippocampal-ATL co-HFOs exhibit an increase in broadband HFA during memory retrieval, which is indicative of heightened broadband neuronal activity in the ATL. Notably, this feature is less prominent for ATL HFOs that were not coincident with an hHFO. Hence, hHFOs are associated with both oscillatory and broadband HFA ATL cortical activity, but synergy between hippocampal-ATL HFOs elicited more cortical activity. Hence, these mechanisms may function in concert to generate periods of heightened hippocampal-cortical network activation. Further, it is interesting that semantic network HFOs do not display a similar increase in broadband HFA like the ATL. To this end, Khodagholy et al. reported that HFOs were not prevalent in the rodent cortex outside of association areas³⁷; hence, it is possible that association cortex HFOs are unique in function compared to HFOs in other cortical areas.

Low-frequency oscillations are thought to bias the activity of larger cortical regions, whereas HFOs engage more specific neuronal ensembles.³⁹ Recent studies have described relationships between HFOs and low-frequency oscillations in the delta^{40,41} and theta^{12,42} frequency ranges. In our study, we found that 3–5 Hz oscillations were more associated with hippocampal-ATL co-HFOs compared to ATL HFOs that were not coincident with an hHFO. These oscillations may generate synergy where cortical assemblies of synchronous low-frequency oscillations and HFOs coordinate the precise activation of cortical ensembles during word list retrieval. Alternatively, it is possible that concerted low-frequency oscillations are underlying core encoding processes and HFOs function as an immediate replay mechanism for heightened memory consolidation. In the context of our findings, hHFOs that “successfully” co-occur with a cortical HFO may be directed by cortical low-frequency oscillations, which more optimally engage the memory network as compared to non-coincident HFOs. Future research with more expansive hippocampal and cortical sampling should further investigate specific regions or networks that exhibit coupling between

low-frequency oscillations and HFOs, as this would support localized cortical function.

HFOs in the 70–180 Hz frequency band encompass a wide range of high-frequency phenomena, including ripple and fast gamma/epsilon activity.^{1,10} Recent human iEEG studies have reported human hippocampal high-frequency bursts in memory tasks as ripple oscillations, akin to the well-established hippocampal sharp wave ripples in rodents. However, sharp wave ripples are thought to predominate in passive, offline states, whereas gamma oscillations occur in active, exploratory states.² Hence, it is perplexing that human hippocampal ripple oscillations have been reported during active, encoding processes at times when other types of HFOs (in this case, gamma oscillations) are expected to predominate.^{3,43} Additionally, sharp wave ripples are thought to be antagonistic to theta oscillations, but we identified a subgroup of HFOs that were associated with theta bursts. Hence, we believe that it is difficult to disentangle ripple oscillations from other types of HFOs in humans without the additional techniques that are more commonplace in rodent studies (e.g., laminar recordings). Furthermore, it is not known how to distinguish pathological from physiological HFOs, including if pathological HFOs exist beyond seizure foci.⁴⁴ This is further complicated by the fact that this study and other similar studies use intracranial electrodes that are placed in locations hypothesized to be within seizure networks. To this end, it is likely that these detected HFOs are physiological because the identified increases in hHFO rate were locked to discrete cognitive events (encoding and retrieval) and linked with memory performance. It is unknown whether pathological HFOs would exhibit such a precise relationship with cognitive processes. Taken together, although this may detract from the relation of our findings to, for example, gamma oscillations in rodents or “non-pathologic” HFOs in participants without epilepsy, we support the use of the broader “HFO” terminology.

In summary, while human participants performed word list learning task, we identified hHFO-associated activation of specific cortical regions that were active during semantic processing during memory retrieval. We observed an interplay between the hippocampus and the ATL where, in times of hHFOs, the ATL exhibits synchronous increases in cortical HFOs and broadband HFA. Co-HFOs across the hippocampus, ATL, and semantic processing areas show specificity based on recall content and may serve as a powerful mechanism for recruitment of specific semantic-memory-containing regions. Further, co-HFOs in the hippocampus and the ATL are more likely to be coincident with cortical low frequency oscillations, suggestive of potential synergy between low-frequency oscillations and HFOs. These findings extend our understanding of word memory retrieval, elucidate the function of the ATL in coordinating activation of semantic processing regions, and provide evidence for HFOs as a mechanism of multi-nodal synchrony in human brain networks that may underlie human advanced cognitive function.

Limitations of the study

There are some limitations of the present study that should be considered when interpreting the findings. First, the locations

of electrode implantation were determined exclusively on clinical grounds by the participants' clinical care team. Hence, coverage across participants was largely heterogeneous, and conclusions could only be drawn for parcellated cortical regions across participants. Furthermore, although several measures were taken to minimize the potential influence of epilepsy pathology on the results, certain factors, such as the effects of medications, could not be entirely ruled out. Next, the methods used in this study cannot establish causal relationships between brain regions. Finally, this study should be replicated with larger cohorts to improve the generalizability of our findings.

RESOURCE AVAILABILITY

Lead contact

Requests for further information and resources should be directed to and will be fulfilled by the lead contact, Akash Mishra (amishra4@northwell.edu).

Materials availability

This study did not generate any new reagents.

Data and code availability

- De-anonymized electrophysiological and behavioral data have been deposited to OSF (<https://osf.io/q52we/>) and are publicly available as of the date of publication.
- All original code has been deposited to OSF (<https://osf.io/q52we/>) and is publicly available as of the date of publication.
- Any additional information required to reanalyze the data reported in this paper is available from the [lead contact](#) upon request.

ACKNOWLEDGMENTS

We would like to thank the participants for volunteering their time and effort to participate in our study. We also thank the Epilepsy Monitoring Unit staff at the North Shore University Hospital for their support throughout the study. We thank Yitzhak Norman and Jose Herrero for providing helpful feedback on the analysis and methods.

Sources of financial support: research reported in this publication was supported by the National Institute on Deafness and Other Communication Disorders (NIDCD) and the National Institute of Mental Health (NIMH) of the National Institutes of Health (NIH) under Award Numbers R01DC019979 (to S.B.) and F30MH139332 (to A.M.). The content is solely the responsibility of the authors and does not necessarily represent the official views of the National Institutes of Health.

AUTHOR CONTRIBUTIONS

Conceptualization, A.M., S.A., and S.B.; methodology, A.M., S.B., and A.D.M.; investigation and data curation, A.M., S.A., E.E., N.M., G.T., and E.F.; formal analysis, A.M. and S.A.; writing—original draft, A.M. and S.B.; writing—review & editing, A.M., S.A., E.E., N.M., G.T., E.F., A.D.M., and S.B.

DECLARATION OF INTERESTS

The authors declare no competing interests.

STAR★METHODS

Detailed methods are provided in the online version of this paper and include the following:

- [KEY RESOURCES TABLE](#)
- [EXPERIMENTAL MODEL AND STUDY PARTICIPANT DETAILS](#)
- [METHOD DETAILS](#)
 - Stimuli and task

- Identification of verbal recall events
- Intracranial recording acquisition and preprocessing
- Electrode registration and localization
- Selection of semantic network contacts
- High-frequency broadband signal and related spectral analysis
- HFO detection
- Spectral analysis and detection of aperiodic oscillatory activity
- Detection of 3–5Hz oscillations
- Peri-event time histograms
- Cross-correlograms
- Temporal resolution of co-HFO events

● QUANTIFICATION AND STATISTICAL ANALYSIS

SUPPLEMENTAL INFORMATION

Supplemental information can be found online at <https://doi.org/10.1016/j.isci.2025.112171>.

Received: September 9, 2024

Revised: December 19, 2024

Accepted: March 3, 2025

Published: March 13, 2025

REFERENCES

1. Kucewicz, M.T., Cimbalnik, J., Garcia, J.S.S., Brazdil, M., and Worrell, G.A. (2024). High frequency oscillations in human memory and cognition: a neurophysiological substrate of engrams? *Brain* 147, 2966–2982. <https://doi.org/10.1093/brain/awae159>.
2. Buzsáki, G., and Silva, F.L. (2012). High frequency oscillations in the intact brain. *Prog. Neurobiol.* 98, 241–249. <https://doi.org/10.1016/j.pneurobio.2012.02.004>.
3. Norman, Y., Yeagle, E.M., Khuvis, S., Harel, M., Mehta, A.D., and Malach, R. (2019). Hippocampal sharp-wave ripples linked to visual episodic recollection in humans. *Science* 365, eaax1030. <https://doi.org/10.1126/science.aax1030>.
4. Buzsáki, G. (1989). Two-stage model of memory trace formation: A role for “noisy” brain states. *Neuroscience* 31, 551–570. [https://doi.org/10.1016/0306-4522\(89\)90423-5](https://doi.org/10.1016/0306-4522(89)90423-5).
5. Vaz, A.P., Inati, S.K., Brunel, N., and Zaghloul, K.A. (2019). Coupled ripple oscillations between the medial temporal lobe and neocortex retrieve human memory. *Science* 363, 975–978. <https://doi.org/10.1126/science.aau8956>.
6. Dickey, C.W., Verzhbinsky, I.A., Jiang, X., Rosen, B.Q., Kajfez, S., Stedelin, B., Shih, J.J., Ben-Haim, S., Raslan, A.M., Eskandar, E.N., et al. (2022). Widespread ripples synchronize human cortical activity during sleep, waking, and memory recall. *Proc. Natl. Acad. Sci. USA* 119, e2107797119. <https://doi.org/10.1073/pnas.2107797119>.
7. Tong, A.P.S., Vaz, A.P., Wittig, J.H., Inati, S.K., and Zaghloul, K.A. (2021). Ripples reflect a spectrum of synchronous spiking activity in human anterior temporal lobe. *Elife* 10, e68401. <https://doi.org/10.7554/elife.68401>.
8. Vaz, A.P., Wittig, J.H., Inati, S.K., and Zaghloul, K.A. (2023). Backbone spiking sequence as a basis for preplay, replay, and default states in human cortex. *Nat. Commun.* 14, 4723. <https://doi.org/10.1038/s41467-023-40440-5>.
9. Norman, Y., Raccah, O., Liu, S., Parvizi, J., and Malach, R. (2021). Hippocampal ripples and their coordinated dialogue with the default mode network during recent and remote recollection. *Neuron* 109, 2767–2780. <https://doi.org/10.1016/j.neuron.2021.06.020>.
10. Kucewicz, M.T., Cimbalnik, J., Matsumoto, J.Y., Brinkmann, B.H., Bower, M.R., Vasoli, V., Sulc, V., Meyer, F., Marsh, W.R., Stead, S.M., et al. (2014). High frequency oscillations are associated with cognitive processing in human recognition memory. *Brain* 137, 2231–2244. <https://doi.org/10.1093/brain/awu149>.

11. Logothetis, N.K., Eschenko, O., Murayama, Y., Augath, M., Steudel, T., Evrard, H.C., Besserve, M., and Oeltermann, A. (2012). Hippocampal-cortical interaction during periods of subcortical silence. *Nature* 491, 547–553. <https://doi.org/10.1038/nature11618>.
12. Canolty, R.T., Edwards, E., Dalal, S.S., Soltani, M., Nagarajan, S.S., Kirsch, H.E., Berger, M.S., Barbaro, N.M., and Knight, R.T. (2006). High Gamma Power Is Phase-Locked to Theta Oscillations in Human Neocortex. *Science* 313, 1626–1628. <https://doi.org/10.1126/science.1128115>.
13. Axmacher, N., Henseler, M.M., Jensen, O., Weinreich, I., Elger, C.E., and Fell, J. (2010). Cross-frequency coupling supports multi-item working memory in the human hippocampus. *Proc. Natl. Acad. Sci. USA* 107, 3228–3233. <https://doi.org/10.1073/pnas.0911531107>.
14. Fedorenko, E., and Thompson-Schill, S.L. (2014). Reworking the language network. *Trends Cognit. Sci.* 18, 120–126. <https://doi.org/10.1016/j.tics.2013.12.006>.
15. Murphy, E., Forseth, K.J., Donos, C., Snyder, K.M., Rollo, P.S., and Tandon, N. (2023). The spatiotemporal dynamics of semantic integration in the human brain. *Nat. Commun.* 14, 6336. <https://doi.org/10.1038/s41467-023-42087-8>.
16. Woolnough, O., Donos, C., Murphy, E., Rollo, P.S., Roccaforte, Z.J., Dehaene, S., and Tandon, N. (2023). Spatiotemporally distributed frontotemporal networks for sentence reading. *Proc. Natl. Acad. Sci. USA* 120, e2300252120. <https://doi.org/10.1073/pnas.2300252120>.
17. Zhu, Y., Xu, M., Lu, J., Hu, J., Kwok, V.P.Y., Zhou, Y., Yuan, D., Wu, B., Zhang, J., Wu, J., et al. (2022). Distinct spatiotemporal patterns of syntactic and semantic processing in human inferior frontal gyrus. *Nat. Hum. Behav.* 6, 1104–1111. <https://doi.org/10.1038/s41562-022-01334-6>.
18. Forseth, K.J., Kadipasaoglu, C.M., Conner, C.R., Hickok, G., Knight, R.T., and Tandon, N. (2018). A lexical semantic hub for heteromodal naming in middle fusiform gyrus. *Brain* 141, 2112–2126. <https://doi.org/10.1093/brain/awy120>.
19. Ruff, I., Blumstein, S.E., Myers, E.B., and Hutchison, E. (2008). Recruitment of anterior and posterior structures in lexical–semantic processing: An fMRI study comparing implicit and explicit tasks. *Brain Lang.* 105, 41–49. <https://doi.org/10.1016/j.bandl.2008.01.003>.
20. Fedorenko, E., Scott, T.L., Brunner, P., Coon, W.G., Pritchett, B., Schalk, G., and Kanwisher, N. (2016). Neural correlate of the construction of sentence meaning. *Proc. Natl. Acad. Sci. USA* 113, E6256–E6262. <https://doi.org/10.1073/pnas.1612132113>.
21. Guo, C.C., Gorno-Tempini, M.L., Gesierich, B., Henry, M., Trujillo, A., Shany-Ur, T., Jovicich, J., Robinson, S.D., Kramer, J.H., Rankin, K.P., et al. (2013). Anterior temporal lobe degeneration produces widespread network-driven dysfunction. *Brain* 136, 2979–2991. <https://doi.org/10.1093/brain/awt222>.
22. Friederici, A.D., Wang, Y., Herrmann, C.S., Maess, B., and Oertel, U. (2000). Localization of early syntactic processes in frontal and temporal cortical areas: A magnetoencephalographic study. *Hum. Brain Mapp.* 11, 1–11. [https://doi.org/10.1002/1097-0193\(200009\)11:1<1::aid-hbm10>3.0.co;2-b](https://doi.org/10.1002/1097-0193(200009)11:1<1::aid-hbm10>3.0.co;2-b).
23. Humphries, C., Love, T., Swinney, D., and Hickok, G. (2005). Response of anterior temporal cortex to syntactic and prosodic manipulations during sentence processing. *Hum. Brain Mapp.* 26, 128–138. <https://doi.org/10.1002/hbm.20148>.
24. Poeppel, D., and Hickok, G. (2004). Towards a new functional anatomy of language. *Cognition* 92, 1–12. <https://doi.org/10.1016/j.cognition.2003.11.001>.
25. Liu, A.A., Henin, S., Abbaspoor, S., Bragin, A., Buffalo, E.A., Farrell, J.S., Foster, D.J., Frank, L.M., Gedakien, T., Gotman, J., et al. (2022). A consensus statement on detection of hippocampal sharp wave ripples and differentiation from other fast oscillations. *Nat. Commun.* 13, 6000. <https://doi.org/10.1038/s41467-022-33536-x>.
26. Sakon, J.J., and Kahana, M.J. (2022). Hippocampal ripples signal contextually mediated episodic recall. *Proc. Natl. Acad. Sci. USA* 119, e2201657119. <https://doi.org/10.1073/pnas.2201657119>.
27. Sakon, J.J., Halpern, D.J., Schonhaut, D.R., and Kahana, M.J. (2024). Human Hippocampal Ripples Signal Encoding of Episodic Memories. *J. Neurosci.* 44, e0111232023. <https://doi.org/10.1523/jneurosci.0111-23.2023>.
28. Buzsáki, G. (2015). Hippocampal sharp wave-ripple: A cognitive biomarker for episodic memory and planning. *Hippocampus* 25, 1073. <https://doi.org/10.1002/hipo.22488>.
29. Mukamel, R., Gelbard, H., Arieli, A., Hasson, U., Fried, I., and Malach, R. (2005). Coupling Between Neuronal Firing, Field Potentials, and fMRI in Human Auditory Cortex. *Science* 309, 951–954. <https://doi.org/10.1126/science.1110913>.
30. Miller, K.J., Honey, C.J., Hermes, D., Rao, R.P., denNijs, M., and Ojemann, J.G. (2014). Broadband changes in the cortical surface potential track activation of functionally diverse neuronal populations. *Neuroimage* 85, 711–720. <https://doi.org/10.1016/j.neuroimage.2013.08.070>.
31. Skelin, I., Zhang, H., Zheng, J., Ma, S., Mander, B.A., McManus, O.K., Vadera, S., Knight, R.T., McNaughton, B.L., and Lin, J.J. (2021). Coupling between slow waves and sharp-wave ripples engages distributed neural activity during sleep in humans. *Proc. Natl. Acad. Sci. USA* 118, e2012075118. <https://doi.org/10.1073/pnas.2012075118>.
32. Helfrich, R.F., Lendner, J.D., Mander, B.A., Guillen, H., Paff, M., Mnatsakanian, L., Vadera, S., Walker, M.P., Lin, J.J., and Knight, R.T. (2019). Bidirectional prefrontal-hippocampal dynamics organize information transfer during sleep in humans. *Nat. Commun.* 10, 3572. <https://doi.org/10.1038/s41467-019-11444-x>.
33. Abadchi, J.K., Nazari-Ahangarkolae, M., Gattas, S., Bermudez-Contreras, E., Luczak, A., McNaughton, B.L., and Mohajerani, M.H. (2020). Spatiotemporal patterns of neocortical activity around hippocampal sharp-wave ripples. *Elife* 9, e51972. <https://doi.org/10.7554/elife.51972>.
34. Rothschild, G., Eban, E., and Frank, L.M. (2017). A cortical–hippocampal loop of information processing during memory consolidation. *Nat. Neurosci.* 20, 251–259. <https://doi.org/10.1038/nn.4457>.
35. Vaz, A.P., WittigJr, J.H., Inati, S.K., and Zaghloul, K.A. (2020). Replay of cortical spiking sequences during human memory retrieval. *Science* 367, 1131–1134. <https://doi.org/10.1126/science.aba0672>.
36. Ralph, M.A.L., Sage, K., Jones, R.W., and Mayberry, E.J. (2010). Coherent concepts are computed in the anterior temporal lobes. *Proc. Natl. Acad. Sci. USA* 107, 2717–2722. <https://doi.org/10.1073/pnas.0907307107>.
37. Khodagholy, D., Gelinas, J.N., and Buzsáki, G. (2017). Learning-enhanced coupling between ripple oscillations in association cortices and hippocampus. *Science* 358, 369–372. <https://doi.org/10.1126/science.aan6203>.
38. Patel, J., Schomburg, E.W., Berényi, A., Fujisawa, S., and Buzsáki, G. (2013). Local Generation and Propagation of Ripples along the Septotemporal Axis of the Hippocampus. *J. Neurosci.* 33, 17029–17041. <https://doi.org/10.1523/jneurosci.2036-13.2013>.
39. Buzsáki, G. (2006). *Rhythms of the Brain* (Oxford University Press). <https://doi.org/10.1093/acprof:oso/9780195301069.001.0001>.
40. Dickey, C.W., Verzhbinsky, I.A., Jiang, X., Rosen, B.Q., Kajfez, S., Eskandar, E.N., Gonzalez-Martinez, J., Cash, S.S., and Halgren, E. (2022). Cortical Ripples during NREM Sleep and Waking in Humans. *J. Neurosci.* 42, 7931–7946. <https://doi.org/10.1523/jneurosci.0742-22.2022>.
41. Kunz, L., Staresina, B.P., Reinacher, P.C., Brandt, A., Guth, T.A., Schulze-Bonhage, A., and Jacobs, J. (2024). Ripple-locked coactivity of stimulus-specific neurons and human associative memory. *Nat. Neurosci.* 27, 587–599. <https://doi.org/10.1038/s41593-023-01550-x>.
42. Tort, A.B.L., Scheffer-Teixeira, R., Souza, B.C., Draguhn, A., and Brankačk, J. (2013). Theta-associated high-frequency oscillations

- (110–160Hz) in the hippocampus and neocortex. *Prog. Neurobiol.* 100, 1–14. <https://doi.org/10.1016/j.pneurobio.2012.09.002>.
43. Chen, Y.Y., Aponik-Gremillion, L., Bartoli, E., Yoshor, D., Sheth, S.A., and Foster, B.L. (2021). Stability of ripple events during task engagement in human hippocampus. *Cell Rep.* 35, 109304. <https://doi.org/10.1016/j.celrep.2021.109304>.
 44. Worrell, G.A., Gardner, A.B., Stead, S.M., Hu, S., Goerss, S., Cascino, G.J., Meyer, F.B., Marsh, R., and Litt, B. (2008). High-frequency oscillations in human temporal lobe: simultaneous microwire and clinical macro-electrode recordings. *Brain* 131, 928–937. <https://doi.org/10.1093/brain/awn006>.
 45. Kollmeier, B., Warzybok, A., Hochmuth, S., Zokoll, M.A., Uslar, V., Brand, T., and Wagener, K.C. (2015). The multilingual matrix test: Principles, applications, and comparison across languages: A review. *Int. J. Audiol.* 54, 3–16. <https://doi.org/10.3109/14992027.2015.1020971>.
 46. Oostenveld, R., Fries, P., Maris, E., and Schoffelen, J.-M. (2011). FieldTrip: Open Source Software for Advanced Analysis of MEG, EEG, and Invasive Electrophysiological Data. *Comput. Intell. Neurosci.* 2011, 156869. <https://doi.org/10.1155/2011/156869>.
 47. Groppe, D.M., Bickel, S., Dykstra, A.R., Wang, X., Mégevand, P., Mercier, M.R., Lado, F.A., Mehta, A.D., and Honey, C.J. (2017). iELVis: An open source MATLAB toolbox for localizing and visualizing human intracranial electrode data. *J. Neurosci. Methods* 281, 40–48. <https://doi.org/10.1016/j.jneumeth.2017.01.022>.
 48. Papademetris, X., Jackowski, M.P., Rajeevan, N., DiStasio, M., Okuda, H., Constable, R.T., and Staib, L.H. (2006). BiolImage Suite: An integrated medical image analysis suite: An update. *Insight J.* 2006, 209.
 49. Fischl, B. (2012). FreeSurfer. *Neuroimage* 62, 774–781. <https://doi.org/10.1016/j.neuroimage.2012.01.021>.
 50. Desikan, R.S., Ségonne, F., Fischl, B., Quinn, B.T., Dickerson, B.C., Blacker, D., Buckner, R.L., Dale, A.M., Maguire, R.P., Hyman, B.T., et al. (2006). An automated labeling system for subdividing the human cerebral cortex on MRI scans into gyral based regions of interest. *Neuroimage* 31, 968–980. <https://doi.org/10.1016/j.neuroimage.2006.01.021>.
 51. Cohen, J. (2013). *Statistical Power Analysis for the Behavioral Sciences* A (Press).
 52. de la Prida, L.M., Staba, R.J., and Dian, J.A. (2015). Conundrums of High-Frequency Oscillations (80–800 Hz) in the Epileptic Brain. *J. Clin. Neurophysiol.* 32, 207–219. <https://doi.org/10.1097/wnp.0000000000000150>.
 53. Gelinas, J.N., Khodagholy, D., Thesen, T., Devinsky, O., and Buzsáki, G. (2016). Interictal epileptiform discharges induce hippocampal–cortical coupling in temporal lobe epilepsy. *Nat. Med.* 22, 641–648. <https://doi.org/10.1038/nm.4084>.
 54. Whitten, T.A., Hughes, A.M., Dickson, C.T., and Caplan, J.B. (2011). A better oscillation detection method robustly extracts EEG rhythms across brain state changes: The human alpha rhythm as a test case. *Neuroimage* 54, 860–874. <https://doi.org/10.1016/j.neuroimage.2010.08.064>.
 55. Kosciessa, J.Q., Grandy, T.H., Garrett, D.D., and Werkle-Bergner, M. (2020). Single-trial characterization of neural rhythms: Potential and challenges. *Neuroimage* 206, 116331. <https://doi.org/10.1016/j.neuroimage.2019.116331>.
 56. Donoghue, T., Haller, M., Peterson, E.J., Varma, P., Sebastian, P., Gao, R., Noto, T., Lara, A.H., Wallis, J.D., Knight, R.T., et al. (2020). Parameterizing neural power spectra into periodic and aperiodic components. *Nat. Neurosci.* 23, 1655–2166. <https://doi.org/10.1038/s41593-020-00744-x>.
 57. Gonzalez, C.E., Mak-McCully, R.A., Rosen, B.Q., Cash, S.S., Chauvel, P.Y., Bastui, H., Rey, M., and Halgren, E. (2018). Theta Bursts Precede, and Spindles Follow, Cortical and Thalamic Downstates in Human NREM Sleep. *J. Neurosci.* 38, 9989–10001. <https://doi.org/10.1523/neurosci.0476-18.2018>.
 58. Jiang, X., Gonzalez-Martinez, J., and Halgren, E. (2019). Coordination of Human Hippocampal Sharpwave Ripples during NREM Sleep with Cortical Theta Bursts, Spindles, Downstates, and Upstates. *J. Neurosci.* 39, 8744–8761. <https://doi.org/10.1523/neurosci.2857-18.2019>.
 59. Scott, D.W. (1979). On optimal and data-based histograms. *Biometrika* 66, 605–610. <https://doi.org/10.1093/biomet/66.3.605>.

STAR★METHODS

KEY RESOURCES TABLE

REAGENT or RESOURCE	SOURCE	IDENTIFIER
Software and algorithms		
MATLAB	Mathworks Inc.	R2023a
Fieldtrip	Oostenveld et al. ⁴⁶	https://www.fieldtriptoolbox.org/
iELVis Toolbox	Groppe et al. ⁴⁷	http://ielvis.pbworks.com/w/page/116347253/FrontPage
FreeSurfer	Fischl ⁴⁹	https://surfer.nmr.mgh.harvard.edu/
Custom MATLAB code	This paper	DOI
Other		
Electrophysiology data acquisition system	Tucker Davis Technologies Inc.	PZ5M
Intracranial electrodes	PMT Corp.	Cortac Grids & Strips; sEEG
Deposited data		
	Open Science Framework	https://osf.io/q52we/

EXPERIMENTAL MODEL AND STUDY PARTICIPANT DETAILS

Intracranial recordings were obtained from nine patients (7 females, median age 32, age range 19–58) with medically intractable epilepsy undergoing iEEG recording at Northwell Health (New York, USA) to assist in the identification of epileptogenic zones for potential surgical treatment. Patients undergo continuous iEEG monitoring for a period of 1–3 weeks, during which they may participate in cognitive and functional testing. The decision to implant, location of implanted electrodes, and the duration of implantation were made entirely on clinical grounds by the treatment team. Participants were selected to participate in this study based on presence of adequate hippocampal and cortical coverage and ability to perform a word list learning task. No exclusions were made regarding a participant's sex, gender, race, ethnicity, or socioeconomic status. Hence, the influence of sex, gender, or both on the results of this study were not assessed, which potentially limits the generalizability of our findings. All participants were over 18 years of age and provided written informed consent to partake in this study. All study procedures were approved by the Institutional Review Board at The Feinstein Institutes for Medical Research.

No clinical seizures occurred during or within the two-hour period prior to the experimental blocks. All participants performed the task in their primary language (English or Spanish) and all participants were found to have left-hemisphere dominance for language identified via Wada testing and language fMRI. Patient information, including number of contacts, region of seizure focus, primary language, and post-implantation treatment are provided in [Table S1](#). Participants were not allocated to a particular study arm, as there was only one experimental group, and no *a priori* sample size analysis was performed.

METHOD DETAILS

Stimuli and task

Construction of word sets: In each trial, twelve monosyllabic English words were selected from a set of words such that they formed a set of three sentences of four syllables each (sentence trials) or a randomized list (non-sentence trials). Sentences had the same syntactic structure: noun + verb + adjectivedescriptor + noun, but each individual word did not have any relation to other presented words (i.e. there was no syntactic dependence among words and participants could not reasonably predict the upcoming word).⁴⁵ Fifteen sentence trials and fifteen non-sentence trials were randomly shuffled to create the thirty trials that composed the experiment. In each trial, the words were presented in an isochronous manner without any acoustic gap between them. Word stimulus onset asynchrony (SOA) was 667ms (1.5 Hz word presentation) for all participants except participants 1 and 2 where the SOA was 500ms (2 Hz word presentation).

Participants were provided with instructions for the task, including a sample set of words, and we adjusted speaker volume for comfort as needed. Each trial started with a participant-initiated button press, and participants waited 500ms before being presented with either a sentence trial or a non-sentence trial. Upon the presentation of the words, participants waited 2000ms before being presented with a distractor task. In the arithmetic distractor task, participants were asked to determine whether a given arithmetic operation was true or false (e.g. “2+94=96” is true and “3+39=41” is false). The operation was visually presented one number or symbol at a time, each presented for 500ms with an inter-trial interval of 400ms. After the final number, participants responded with a button press. In each trial, participants were presented two equations in succession. Following this, participants viewed a screen where they

were asked to verbally recall as many words as they could from the twelve words that were presented earlier in the trial without any prompts or cues (hence, free recall). Participants pushed a button to designate that they were done recalling and were ready for the next set of words (in the next trial) to begin. For participant 3, immediately after the presentation of words, we asked the participant to recall as many words as they could to establish adequate comprehension of words. If the participant was unable to verbally recall any of the words from the presented set, we manually aborted the trial and the next trial began. If the participant was able to recall any words, the trial continued. Two out of thirty trials were manually aborted. For participant 7, the task was conducted using Spanish stimuli.

We executed this task using the Psychophysics Toolbox in MATLAB (MathWorks Inc., Natick, MA, USA). Visuals were presented using a 15" laptop or 24" monitor with sound stimuli sampled at 44.1k Hz. Sound stimuli were presented with a speaker located directly in front of the participant. To minimize distractions and external noise, all other electronic devices in the study room were switched off, we kept the experiment room door closed, and clinical staff were instructed to try to not enter or exit the room during the duration of the task.

Identification of verbal recall events

A microphone affixed to a nearby stable surface recorded the entire experimental block, including the free recall periods for each trial. The onsets and offsets of each recall event and the contents of the recall were extracted in an offline analysis using Audacity auditory presentation software (Audacity, Oak Park, MI, USA). Recall events were designated as any relevant words that the participant stated, and we marked any recall onset that occurred longer than 4 seconds after the offset of the previous recall event as an independent event. Any trials induced by a mis-click or that included outside interference were removed from subsequent analysis.

To quantify the number of recalled words, we performed a median split by participant across all trials. Based on whether the participant was able to recall more than or less than the median, we marked each trial as "effective" recall or "poor" recall, respectively. This aimed to normalize for variation in the number of recalled words per participant.

Intracranial recording acquisition and preprocessing

Intracranial recording sites were subdural grids, strips, stereo-EEG depth electrodes, or a combination thereof (Ad-Tech Medical Instrument Corp., Oak Creek, WI, USA; Integra LifeSciences, Princeton, NJ, USA; PMT Corp., Chanhassen, MN). Recording sites in the subdural grids and strips were 1- or 3-mm platinum disks with 4- or 10-mm intercontact (disk center to disk center) spacing. Recording sites in depth electrodes were 2-mm platinum cylinders with 0.8mm diameter and 4.4-mm intercontact spacing. During the recordings, we re-referenced the intracranial EEG signal to a subdermal electrode or subdural strip. Neural signals were acquired using a Tucker-Davis Technologies (TDT) PZ5M module (Tucker-Davis Technologies Inc., Alachua, FL) at either 1.5- or 3k Hz and saved for offline analysis. Prior to experimentation, signal quality and power spectra were inspected online using TDT Synapse oscilloscope software, and if needed, changes were made to improve signal quality. During the task, transistor-transistor logic pulses triggered by the stimulus presentation software were generated at specific experimental timepoints of interest (onset of each trial, onset of the distractor task, and onset of free recall cue). This served to synchronize intracranial recordings to the task-related events of interest.

We performed all data analysis in MATLAB using FieldTrip⁴⁶ and custom written scripts. We resampled neural data to 500 Hz, and we removed potential 60 Hz (and its 120 and 180 Hz harmonics) power-line noise using a notch filter (zero-lag linear-phase Hamming-window FIR band-stop filter). We visually inspected raw iEEG data to detect noisy or bad channels, which were excluded from further analysis. Then, we average referenced neural data to remove global artifacts. Seizure onset channels identified by the clinical team were excluded from analysis.

Electrode registration and localization

For each participant, a pre-implant T1w structural MRI and post-implant CT scan were collected. We performed intracranial electrode localization using the iELVis toolbox,⁴⁷ which utilizes Biolimage Suite,⁴⁸ FreeSurfer,⁴⁹ and custom written code. To summarize the electrode localization procedure, electrode contacts were manually registered in the post-implantation CT scan using Biolimage Suite, which is co-registered to the pre-implantation MRI scan to minimize localization error due to brain shift. We used FreeSurfer to align the participant's pre-implantation MRI to a standard coordinate space, segment the cortical surface, assign anatomical locations for each contact, and determine hippocampal subfields in each participant. Next, we used iELVis software to project the contact locations onto a FreeSurfer standard surface. We visually inspected the location of these contacts on the participant's brain to confirm contact location.

Selection of semantic network contacts

We determined electrode preference based on whether HFA increased significantly during the presentation window. We followed the methodology implemented by Fedorenko et al. in a previous study.²⁰ Sentence-responsive contacts were defined as contacts in which the magnitude of HFA was significantly higher for trials in the sentence condition compared to the non-sentence condition; contacts for which the effect was in the opposite direction were classified as non-sentence responsive. To identify the functionality and specificity in responsiveness across contacts, we constructed a 500 ms epoch of HFA for each presented word, with the epoch beginning at the onset of each presented word and ending 50ms prior to the onset of the next word, and we classified each epoch as

being part of a sentence trial or a non-sentence trial. We then baseline corrected the signal using a 450ms pre-trial baseline (we removed 50ms to account for any residual activity from the previous stimulus). For each electrode, we then computed the mean HFA across the twelve-word positions in each trial for each condition. We then performed a Spearman's correlation between the single trial mean HFA and a vector of condition labels (sentences = 1; non-sentences = -1). To assess the significance of this correlation, we compared the resulting correlation coefficients (Spearman's rho) against a null distribution obtained by randomly reordering the condition labels and calculating a new Spearman's rho for 1000 iterations. Correlations that were in the top or bottom 2.5% of the distribution were denoted as significant. Significant contacts with a positive rho value (that is, a positive correlation) were marked as sentence-responsive, and significant contacts with a negative rho value were marked as non-sentence-responsive. Hence, the semantic network was divided into contacts that were preferentially sentence-responsive and contacts that were preferentially responsive to non-sentence trials. Separately, contacts that showed increases in HFA for both sentence and non-sentence trials as compared to baseline were marked as general language-responsive.

We also identified contacts that were in the anterior temporal lobe. To systematically define these contacts, we identified the axis between the most anterior tip of the temporal lobe to the most posterior aspect of the middle temporal lobe as defined by the Desikan-Killiany atlas⁵⁰ overlaid onto each participant's specific brain image. All contacts that were anterior to the orthogonal line constructed at one-third of the constructed temporal lobe axis were defined as being in the ATL.

High-frequency broadband signal and related spectral analysis

We defined HFA signal as the mean normalized power of 70–150 Hz. For analyses in which spectrograms were computed or HFA activity was compared between contact types, we computed HFA power independently for each contact by: (1) bandpass filtering the iEEG signal in 10 Hz bands (i.e. 70–80 Hz, 80–90 Hz, 90–100 Hz, and so on, but excluding windows of 118–122 Hz to exclude potential power line noise) using a fourth-order Butterworth filter; (2) applying a Hilbert transform to each individual frequency band and taking the absolute value of the resulting envelope; (3) amplitude normalization, via division of the mean of the frequency band signal; (4) averaging all normalized frequency band envelopes. This procedure results in a single time series that serves as a proxy for mean neuronal activity at a given contact. This normalization procedure has been implemented previously³ and corrects for the 1/f decay in EEG power spectra while providing temporal smoothing at the higher frequencies. Prior to any analysis implementing this derived HFA signal, we visually inspected the data for artifacts. Candidate artifacts were identified as peaks 4 standard deviations above the mean HFA signal across contacts. Artifacts were then visually inspected, and if needed, contacts were marked to be excluded from any additional analysis.

Epochs of HFA signal were created as needed for time periods of interest, including HFO-locked, response time-locked, and word presentation-locked. For each, we normalized the HFA signal with a pre-event baseline (450ms pre-trial baseline or, for HFO-locked analyses, a 500ms period prior to the HFO). This allowed for the comparison of contacts within regions of interest across participants. To compare HFA across two signals of interest, we implemented a two-tail nonparametric cluster-based test (clustering across time bins) using the fieldtrip toolbox.⁴⁶

To examine the effect size of HFA effects, we used a Cohen's d statistic. We evaluated the effect size as the following: small ($d=0.2$), medium ($d=0.5$), and large ($d=0.8$).⁵¹ We implemented this metric when determining the magnitude of effect, by electrode, for (1) preferred and non-preferred analysis (averaging over a 500ms epoch around hHFO peak for each) and (2) examining peri-hHFO HFA compared to baseline (comparing 500ms epoch around hHFO peak with a 500ms period preceding this).

HFO detection

We performed an offline HFO detection that closely aligns with methodology utilized in a prior study.³ We elected to detect HFOs in a 70–180Hz frequency range because this encompasses the 80–140Hz “ripple-band” and 80–150Hz “fast gamma/epsilon-band” that have been previously studied and reported.¹ This also aligns with the frequency range known to be associated with synaptic transmission.⁵² Demonstration of the peak HFO frequencies show that most detected HFOs contain a peak frequency within the 80–140 Hz range (Figures 1F and 4F).

For hHFO detection, we identified an electrode contact located in or adjacent to the lateral aspect of the body of the hippocampus (in the region of the CA1 subfield). We then verified the exact anatomical location of electrode selection (Figure S1). We re-referenced the signal to the closest nearby white matter contact, 8.8mm away from the selected hippocampal contact and filtered between 70 and 180 Hz using a zero-lag, linear-phase Hanning window FIR filter with 5 Hz transition band. We then applied a Hilbert transform to attain signal amplitude. Then, we clipped this signal to 3 standard deviations to minimize bias that may arise from high HFO rates. The clipped signal was then squared and smoothed via a Kaiser-window FIR low-pass filter with 40 Hz cutoff. To attain a baseline for event detection, we used the mean and standard deviation of the pre-experiment resting period signal after removal of 100ms periods surrounding any manually-detected IEDs (please see below for methodology and rationale). Events from the original signal that exceeded 3 standard deviations above baseline were selected as candidate HFO events. We defined the onset and offset of each event as the timepoints where the HFO frequency-band power decreased below 2 standard deviations. Events shorter than 42ms (computed as the duration of 3 cycles of 70 Hz) and longer than 250ms were removed. Events where the peak-to-peak difference was under 200ms of one another were merged. We then aligned the HFO peak to the maximum amplitude of the HFO frequency-band envelope.

To control for global and transient artifacts, we performed a HFO detection on the common average signal of all contacts. Any HFO events that occurred within 50ms of a common average HFO frequency-band peak were removed. To avoid inclusion of any pathological high-frequency discharges, specifically inter-ictal discharges (IEDs), we implemented an automatic IED detection method; the raw hippocampal bipolar LFP was filtered between 25-60 Hz (using a zero-lag, linear-phase Hamming window FIR filter) and we applied a similar methodology to the HFO detection described above (rectifying, squaring, normalizing). Detected events that exceeded 5 standard deviations were marked as IEDs. For hHFOs, we also used a manual detection process. Candidate IEDs were identified as having an amplitude greater than 4 standard deviations above mean, and a peak width of less than 100ms. Of these candidates, true IEDs were manually selected based on patient-specific IED physiology. All HFO events occurring within 200ms of an IED event were rejected.⁵³ Finally, we confirmed whether detected HFOs were true oscillations by using the eBOSC toolbox.^{54,55} We mandated that all identified events had at least one oscillatory cycle within the HFO frequency range.

We assessed hHFOs during perception of word list, during which participants listened to the word list, and recall, within four-second windows around the onset of independent verbal recall events (defined as verbal recall events that were at least four seconds apart). This aimed to maximize the potential that hHFO events were directly involved in the encoding and recall process.

Spectral analysis and detection of aperiodic oscillatory activity

We then evaluated whether the increases in hHFO-associated ATL HFA were increases in broadband HFA or cortical HFOs. As HFOs are rhythmic phenomena, if cortical HFOs were indeed driving this effect, we would expect to identify an increase in oscillations detected within the HFO frequency range. We performed a wavelet-based frequency analysis for the 10-200 Hz frequency range (in 1-Hz steps; width 8 Hz) for each detected ATL HFO. We removed 6 Hz bands centered on 60, 120, and 180 Hz to correct for line noise. We then separated all ATL HFO that occurred within 100ms of a hHFO and compared the log-frequency spectrograms for ATL HFOs that were coincident with a hHFO and isolated ATL HFOs without a coincident hHFO. We implemented a cluster-based permutation test to determine significant frequency clusters.

To more closely assess the relationship between ATL HFOs and low-frequency oscillatory phenomena, we performed a wavelet-based frequency analysis for the 1-12 Hz frequency range (in 0.1 Hz steps; width 6 Hz) for each detected ATL HFO. To visualize the changes in lower frequencies, we constructed plots depicting log-power as a function of frequency (averaging over a 500ms window around ATL HFO peak) and power as a function of time. We separated these plots between hHFO-coincident and non-hHFO-coincident ATL HFOs to assess for differences between the two. We confirmed these findings by implementing the FOOOF algorithm (version 1.0.0),⁵⁶ which assists in the decomposition of a neural signal into a periodic and aperiodic component on the single-trial level. We detected low-frequency oscillations in the 2-10 Hz range on peri-ATL HFO data (400ms epoch). We selected the minimum peak height to be 0.3 and the peak width limits were set to be 1-12 Hz. The resulting identified peaks were then plotted onto a histogram to depict most prominent ATL HFO-associated low frequency oscillations.

Detection of 3-5Hz oscillations

We performed low frequency oscillation detection in similar fashion to prior studies.^{57,58} We applied a zero-phase shift 3-5 Hz band-pass filter to the single-channel (cortical contact) LFP data. We set a channel-specific cutoff at 3 standard deviations above the mean and was applied to each channel's Hilbert envelope to identify peaks of theta oscillations. We identified the start and stop of each oscillation event as when the power dropped below 1 standard deviation above the channel mean. Low frequency bursts were included for analysis if their durations fell within 375 and 1000ms (defined as 3 cycles of 8 Hz and 3 Hz, respectively).

Peri-event time histograms

To construct peri-event time histograms across experimental conditions, we used a bin width advised by Scott's optimization method, which optimizes bin size to event density.⁵⁹ For PETH locked to sentence onset, we assessed all hHFOs in the -0.5 to 10 second window relative to onset of word list presentation and utilized an optimized bin size of 200ms with 7-point smoothing. To determine significant time bins, 5000 iterations of peri-presentation onset time histograms were computed by circularly jittering hHFO times across the two-second post-word list presentation window. This enabled us to maintain statistical power despite a low number of hHFO events. We performed a permutation test determine significant time windows. Time windows that were in the top or bottom 2.5% of the distribution (thus implementing an alpha-value of 0.05) were denoted as significant. A similar approach was taken for the peri-verbal recall PETH, but here, statistical power was computed by circularly jittering hHFO times 5000 times across the same -4 to 1 second window relative to onset of verbal free recall (while implementing 90ms bin size with 7-point smoothing). Finally, to compare PETH around the onset of effective vs poor recall periods, we assessed the same -4 to 1 second window with identical 230ms and 4-point smoothing for the two PETH. To determine significance, we shuffled labels of effective and poor recall and generated a distribution of mean hHFO rate differences (5000 iterations). This generated a distribution by which we identified significant timebins.

Cross-correlograms

To examine co-HFOs between two brain regions, we used a methodology by Vaz et al.⁵ and the HFO peak time index to produce cross-correlograms. For each cortical electrode, we computed a cross-correlation between detected hippocampal and cortical HFOs. We pooled these cross-correlations across trials for each electrode pair in each participant, which creates a single cross-

correlogram for each pair of contacts. We normalized the amplitude of each cross-correlation by the duration of the time window of interest and number of electrode pairs such that values represented coincidences per second. For this analysis, we implemented 10ms bins. To determine significance of synchronous HFO events, we jittered cortical HFO event timing and constructed a new cross-correlogram. We repeated this procedure 5000 times and used it to generate a null distribution for a permutation test. We applied this procedure separately for ATL and semantic network contacts.

Temporal resolution of co-HFO events

To determine the temporal resolution of co-HFO events relative to verbal recall onset, we implemented proportions to normalize for the increase in hHFO events that occurs prior to verbal free recall. That is, instead of quantifying the rate of co-HFO events, we quantified the chance that a hHFO event was coincident with a ATL HFO event prior to verbal free recall. We defined a co-HFO event as two HFO events where the peak-to-peak duration was less than 100ms (defined as half of the 200ms maximum HFO duration), as the peak of HFO events are more readily detectable compared to the onset/offset (which differs depending on manually-defined thresholds). We constructed a PETH for the -4 to 2 second window relative to verbal recall onset implementing 300ms bins with 8-point smoothing. To determine significance across timebins, we jittered cortical HFO event timing and constructed a new PETH. We repeated this procedure 5000 times to create a null distribution for a permutation test.

QUANTIFICATION AND STATISTICAL ANALYSIS

For all statistical tests described in this study, an alpha-value of 0.05 was implemented to determine significance. For nonparametric tests comparing two sample medians, Wilcoxon rank-sum z (as the distribution of the U statistic approaches a normal distribution for larger sample sizes) are presented, except for group-level analyses (sample sizes of less than 10), where Mann-Whitney U statistics are presented. Wilcoxon signed-rank W statistics are presented for comparison of medians between paired samples. This information can be found for each statistical test within the [results](#) section and/or associated figure legends.